Signal band estimation of the Blackfoot 3C-3D experiment.

Alana R. Schoepp, Gary F. Margrave, The CREWES Project

ABSTRACT

The spectral content of the Blackfoot 3C-3D was analyzed through the application of the f-x method. This method is used for the estimation of signal band of multichannel reflection data. Signal is manifest through the lateral continuity of events, while noise causes lateral incoherence. The method is first demonstrated on several synthetic examples, and then applied to the Blackfoot 3C-3D seismic survey. Estimation of the signal bandwidth in the survey is complex, as the line was processed separately by two different companies, Pulsonic Geophysical Ltd. and Sensor Geophysical Ltd. The P-P data was found to contain frequencies ranging from 10 to 80 Hz, however the radial spectral content was lower, as expected, ranging from approximately 5 to 30 Hz. Migration increased the apparent signal band of the stack; however it also created spectral coherence at frequencies which were completely incoherent in the stacked section. The Pulsonic processed data had greater spectral coherence and similar bandwidths as compared to the Sensor processed data.

INTRODUCTION

The Blackfoot 3C-3D broad-band experiment was conducted in November 1996 over the Blackfoot field (southeast of Strathmore, Alberta, Canada, and owned by Pan Canadian Petroleum Ltd.) The survey was shot as a single patch approximately 3.5 km by 2.5 km in size. There were 630 receiver positions, spaced 60 meters apart and the receivers lines were separated by 255 meters. The 10 Hz 3-C phones (Geospace LRS) were deployed as single phones at each station. Offsets reached a maximum of 4300 meters. Source effort was a 4 kg dynamite charge at 18m depth. Sources were also spaced 60 meters apart with 210 meters separating source lines Recording length was 4 seconds and the data was sampled at 2 ms. Recording was done under contract by Veritas Geophysical Ltd using the I/O System II. (See Stewart et al. 1996 for more information on the Blackfoot experiments.)

Since the temporal and spatial resolution of reflection seismic data is directly dependent on spectral bandwidth, the estimation and enhancement of the signal band is a central problem in the production of optimal seismic images. Reliable signal band estimation can guide the application of spectral enhancement techniques and also provides an objective basis for the comparison of different processing sequences or acquisition parameter tests. Many signal estimation methods are related to the notion of semblance and, though useful, are problematic. Semblance (see Yilmaz 1987, Neidell and Taner 1971) identifies signal by assuming it to have spatial coherence along some trajectory in either time or frequency. Frequency domain semblance estimates are computed as the ratio of the Fourier amplitude spectrum of the average of the traces in a ensemble divided by the average of the Fourier amplitude spectra of that ensemble. The numerator of the semblance calculation is assumed to estimate signal while the denominator estimates signal plus noise. Thus semblance estimates a number between 0 and 1 (as a function of frequency) with zero indicating no signal and 1 indicating no noise. Though useful, semblance is strongly dependent on the alignment of signal in the ensemble and the ability of a computer algorithm to detect and sum along that alignment.

An alternative technique is useful here and is essentially the simple display of appropriately computed Fourier spectra. As an example, Figure 1-A shows the "final" cmp stack (not migrated) of the Blackfoot 2D10 Hz array data while figures 1-B and 1-C show f-x amplitude and "complex phase" spectra computed over the time zone indicated in 1-A. (The precise meaning of the complex phase spectra is discussed in the theory section.) The signal band is directly estimated from these displays by visual, interpretive inspection. (In all f-x spectral plots in this paper, the vertical axis is ordinary temporal frequency measured in Hz.) The amplitude spectra are plotted without decibel (db) conversion such that the maximum power is full black and indicate the frequency band over which the stacked section has good spectral power. Signal causes frequency coherence in both amplitude and phase though it is generally easier to see in the phase display. The signal band is thus estimated from the phase spectrum as between roughly 5 and perhaps 100 Hz between stations 101 and 120 and decreases elsewhere to about 5 to 85 Hz. As can be seen, there is a strong correlation between the local topography (1-D) and the signal band and the lateral variation of signal is probably controlled by the near surface geology. The dramatic low power zone near 60 Hz extending from station 140 to 270 on the amplitude spectra is likely a spectral notch due to a near surface source ghost. As is easily demonstrated (e.g. Hatton et al. 1986) a ghost causes a spectral notch at a frequency $f_g = v_w/(2\Delta z)$ where v_w is the weathering velocity and Δz is the source depth. The valley floor had a lower weathering velocity sufficient to cause the ghost notch to move into the spectrum while in the higher terrain it is presumably above 100 Hz. Close inspection of 1-A shows that the ghost notch manifests as lower resolution in the time domain.

THEORY

The computation of f-x spectra for signal band analysis is simple though slightly different from conventional Fourier approaches. First, a nominal temporal window is defined to span a zone of interest. Then the actual length of the window is allowed to fluctuate randomly with each trace while remaining centered on the middle of the time zone. This is done because the use of a spatially invariant window induces a phase coherence which tends to broaden the apparent coherent phase zone leading to overly optimistic signal band estimates (figure 3). If $\Psi(x,t)$ represents the ensemble of seismic traces to be analyzed and $W(x,t)$ is the ensemble of randomly varying windows, then the F-X spectra are given by:

$$\phi(x,f) = \int_{t\,min}^{t\,max} \Psi(x,t) W(x,t) e^{-i2\pi ft} dt \qquad (1)$$

The actual shape of the window function is optional but in all work in this paper it was a boxcar with raised cosine tapers on either end. It is convenient to allow the magnitude of the random fluctuation of window length and the length of the window taper to be programmable parameters expressed as a percentage of the nominal window length. Aside from these windowing details, (1) is a conventional Fourier transform over time of each trace in the ensemble. The amplitude spectra shown in figure 1-B are computed in the standard way from:

$$\text{AMPLITUDE SPECTRA} = |\phi(x,f)| = \sqrt{\text{Re}(\phi(x,f))^2 + \text{Im}(\phi(x,f))^2} \qquad (2)$$

The "phase" spectra are computed in a non-conventional way and will be called "complex phase" spectra:

$$\text{COMPLEX PHASE SPECTRA} = \frac{\phi(x,f)}{|\phi(x,f)|} = \cos(\theta) + i\sin(\theta) \qquad (3)$$

So the display in figure 1-C called "complex phase" is actually the complex spectrum divided by its magnitude. Real and imaginary parts are simply displayed as consecutive samples on a real trace of twice the number of samples as the traces in the amplitude spectrum. This display is preferred to the display of phase angle because phase wrapping can cause apparent trace to trace phase discontinuities which are not a function of signal strength and thus gives a misleading impression of spectral discontinuity. Complex phase contains the same information as conventional phase and has the intuitive interpretation of being a "perfectly whitened" spectrum.

The expectation that spectral coherence indicates signal while the absence of coherence is noise, constrains the nature of the seismic trace ensembles that are amenable to this analysis. Clearly raw shot records contain a great deal of coherent energy that is usually regarded as noise (refractions and surface waves) while much signal energy cannot be expected to appear coherent due to unresolved statics and moveout. CMP stacked sections are better candidates because the coherent noise has largely been surpressed and the reflection signals have been aligned. It is desirable to perform the f-x analysis on stacked data before running any multichannel processes that operate along the midpoint axis. Such post-stack processes as f-x spatial prediction, f-k filters, and migration all tend to correlate the noise portion of the spectrum and lead to biased estimates. Prestack multichannel processes run along the shot, receiver, or offset axes are generally acceptable prior to f-x analysis on CMP stacks. These considerations suggest that CMP stacks without poststack processing are the ideal ensemble for f-x analysis. Thus f-x analysis can be regarded as estimating the "realized" signal band as determined by the entire prestack processing flow.

SYNTHETIC EXAMPLES

Figure 3 shows f-x amplitude and complex phase spectra for a monochromatic (30 Hz), noiseless synthetic. On the left (2-A and 2-C) are results using a spatially constant window while on the right (2-B and 2-D) random windowing was used with a 20% variation in window length. Since the windowing process is a multiplication it must correspond to a convolution of spectra in the frequency domain. Thus the analysis of spectral coherence will always be a mixture of both data and window coherence. Without random windowing, there is apparent signal (phase coherence) (2-C) at all frequencies even though the signal only existed at 30 Hz. Essentially random windowing destroys the phase coherence of the window so that the visible coherence tends towards that of the signal. Of course, the undesirable phase coherence in 2-C is associated with small amplitudes so if this analysis is repeated with a noisy, monochromatic signal, the effect of the random windowing is less dramatic but still desirable.

Figure 4 illustrates the analysis of a broadband synthetic in noise. Each time domain trace consists of a random time series convolved with a wavelet representing signal plus a second random time series of lower mean amplitude representing noise. The signal component is identical for all traces while the noise is a different random sequence for each trace. By construction, the signal band is about 12-62 Hz as indicated in 3-B. In the left column are results for the case of an Ormsby wavelet with flat passband. The label "optimally resolved" is meant in a qualitative sense and refers to an assessment that the signal band, as deduced from the complex phase spectrum (3-D), coincides with the band of strong spectral power as inferred from the

amplitude spectrum (3-C). In the right column, the synthetic has been convolved with a zero phase shaping filter to produce an "under resolved" case. As is evident from the complex phase spectrum, the signal band is the same as on the left, but the amplitude spectrum shows insufficient power in the higher portion of the signal band. When this situation is encountered with real data, it indicates a need for further spectral whitening.

Figure 5 shows that the f-x technique performs well even in the non-stationary case. Here a stationary synthetic (4-A) was created as described in the preceding paragraph except that a much broader band wavelet (15-180 Hz) was used (4-C). The non-stationary synthetic (4-B) was created from the stationary one by subjecting the signal to a time and frequency dependent exponential decay while the noise remained stationary. The exponential decay was essentially a zero phase forward Q operator with Q of 50. (that is $\exp(-\pi ft / Q)$ was applied to the signal component.) As is evident in 4-C, the stationary synthetic has a noise component that is 25-30 db down from the signal. Therefore, constructing frequency dependent decay curves (D) and observing the time at which a particular frequency has decayed by 25-30 db allows the expected non-stationary signal band to be estimated. Thus, as shown in (D), the upper limit of the signal band is expected to be above 160 Hz from 0 to .4 sec, around 70 Hz from .6 to 1.0 sec, and near 40 Hz from 1.2 to 1.6 sec. The f-x analyses in these time zones can be seen to estimate the signal band quite well. Experience has shown that good estimates can be made in fairly small time zones with as little as a few hundred time samples (.3 second windows on 2 mil data are quite feasible). These results exhibit spectral decay very similar to that found in real data (see the next section). The high frequency decay of spectral amplitude with increasing time is paralleled by a similar decay in the bandwidth of phase coherence.

FURTHER APPLICATION TO BLACKFOOT

We will be comparing the 3C-3D signal band to that of the 2D broadband data. The latter was fully examined by Margrave (1995) and two stationary examples are included in this paper. Figure 1 shows the spectral analysis of the P-P data over a time window of 0.2 to 1.6 seconds, and figure 2 shows the bandwidth of the P-S data over a time window of 0.2 to 2.6 seconds. The exploration target is the glauconitic sandstone which occurs at roughly 1.1 seconds in the P-P data and 1.7 seconds in the P-S data.

To examine fully the signal bandwidth of the 3C-3D, several different comparisons were made. The Blackfoot 3C-3D survey was processed by two different companies, Pulsonic Geophysical Ltd. and Sensor Geophysical Ltd. A detailed description of the processing can be found in Simin et al. (1996). A major difference in processing was that Pulsonic processed the entire data set, while Sensor processed the northwest section. There were important additional differences in static solutions, deconvolution, and migration which led to a difference in spectral content. An inline (number 65 striking E-W) and a crossline (number 34 striking N-S) from each processing flow were selected for analysis, and the P-P and P-S data were compared, in each case, both before and after migration. Only the inline spectra are included in this paper, as there was no appreciable difference in the inline and crossline bandwidths. Although migration is expected to bias f-x estimation, analysis of the migrated sections are included as it is difficult to assess the signal to noise reduction effects of the 3D migration relative to the 2D. It is well appreciated that low fold 3D data often gives a superior image to high fold 2D data because diffraction summation along a hyperbolic sheet gives far greater noise reduction than along a 2D hyperbola.

Figures 6 through 9 show the stationary spectral analysis of the Blackfoot 3C-3D. The P-P data as processed by Sensor is displayed in figure 6, and figure 8 contains the same data but processed by Pulsonic. Figure 7 shows the P-S data from Sensor and the same data, processed by Pulsonic is shown in figure 9. The P-P spectra are computed over a time gate of 0.2 to 1.6 seconds, and the P-S spectra are computed over a longer time gate of 0.2 to 2.6 seconds. On the left side of each figure, labeled A to C, is the time display, f-x spectrum and complex phase spectrum of the stacked section, and beside it are similar displays, labeled D to F of the migrated data. The images labeled 'stacked' are fully processed to stack without any poststack processing, whereas the images labeled 'migrated' have been through poststack time variant spectral whitening, f-x signal enhancement (Abama, R., and Claerbout, J., 1995) and migration.

Poststack processing appears to have extended the bandwidth considerably in each case. However, any signal in the migrated spectra that does not correspond to even a faint signal in the stacked spectra should be treated with caution. Migration can strengthen existing signal; however if continuity appears in the migrated spectra that is completely absent from the stacked spectra, it may be an artifact of the processing. Since migration can be viewed as a process of replacing each stacked trace by a wavefront, it must induce a trace-to-trace correlation in the entire frequency spectrum. Since, the spatial extent of the migration wavefront increases with migrated time, we expect this systematic bias to do likewise.

The analyses in the previous figures are over a long time gate and greater insight can be gained from a non-stationary analysis. Figures 10 to 17, each break the previous analysis into three equal zones. The Sensor processed data is shown in figures 10 to 13, while 14 to 17 display the Pulsonic processing. The lower frequency resolution caused by the use of smaller time windows as is characterized by the 'uncertainty principle' is obvious in these figures. Although a decay of frequency with time is apparent in the 2 D data (Margrave 1995), it is not seen in the 3D data. We attribute this difference to the stacking fold in 2D versus 3D data. The source spacing in 3D geometries is typically much larger than in 2D and the result is that the true fold is much more strongly time variant in the 3D than the 2D.

When the displays of the vertical component data are compared, the data appears to have a bandwidth from approximately 10 to 80 Hz. Although the spectra are broadly similar for both processing flows, the Pulsonic processing led to greater spectral coherence on the stacked spectra. The dramatic increase in apparent signal band after migration on the Sensor data is attributed to the aggressive use of time variant spectral whitening and f-x spatial prediction. The signal in the shallow time zones seems to be quite weak in the unmigrated section, but is improved with migration. This is a similar bandwidth as the Blackfoot 2D seismic data.

The radial components of the 3C-3D were processed for converted wave energy with good results. The signal bandwidth ranges from approximately 5 to 30 Hz. There is a more pronounced difference between the two processing results as the Pulsonic processing has greater spectral coherence in all three time zones and a greater bandwidth in the shallow time zone. The 2D Blackfoot survey has considerably wider bandwidth, 5 Hz to 40 Hz. The P-S sections achieved signal bandwidths of about half that of the P-P sections, which is not uncommon.

The Pulsonic processing flow on the stacked data appears to be superior to the Sensor processing flow. The events in all cases have greater spectral coherence as can be seen by the greater degree of continuity. The better estimates from the

migrated sections have been processed by Sensor. However, we are suspicious of these estimates because the poststack processing biases the estimates, also the interpretability of the Sensor data is less (Yang et al., 1996).

SUMMARY AND CONCLUSIONS

The investigation of the Blackfoot 3C-3D experiment indicates a P-P reflection signal band which tops out near 80 Hz in the zones of interest and probably extends below 10 Hz on the low end. The P-S signal band is roughly half the P-P with a high frequency limit of approximately 30 Hz. Migration strengthened the signal coherence in both types of data and seemed to extend the bandwidth, although we are skeptical of the latter result. The signal band is strongly time variant, being quite narrow in the shallow section and inceasing to a maximum in the target zone. This behaviour is opposite to that predicted by simple attenuation concepts and is probably a consequence of the time variance of the 3D fold. The stacked data processed by Pulsonic shows stronger signal than the data processed by Sensor.

ACKNOWLEDGMENTS

We wish to thank Chevron Corporation for allowing this method to be published and the sponsors of the CREWES project for their financial support of this work. We also thank our fellow scientists in the CREWES project for their work with the acquisition, processing, and interpretation of the Blackfoot data.

REFERENCES

Abama, R., and Claerbout, J., 1995, Lateral prediction for noise attenuating by t-x and f-x techniques: Geophysics, 60, 1887-1896

Foltinek, D. S., Bland, H. C., 1996, 1996 CREWES Software Release: CREWES 1996 Research Report

Hatton, L, Worthington, M., Makin, J, 1986, Seismic Data Processing - Theory and Practice, Blackwell Scientific Publications

Hendrick, N. and Hearn, S., 1993, Evaluation of Seismic Trace Inversion Techniques, Exploration Geophysics, 24, 549-560

Kjartannson, E, 1979, Constant Q wave propagation and attenuation, J. Geophys. Res., 84, 4737-4748

Margrave, G. F., 1995, Estimates of the Signal Band of the Blackfoot Broad-Band Data: CREWES 1995 Research Report

Neidell, N.S., and Taner, M.T., 1971, Semblance and other coherency measures for multichannel seismic data, Geophysics, 34, 482-497

Oldenburg, D.W., Scheuer, T., and Levy, S., 1983, Recovery of the acoustic impedance from reflection seismograms, Geophysics, 48, 1318-1337

Simin, V., Harrison M. P., Lorentz G. A., 1996, Processing the Blackfoot 3C-3D Seismic Survey: CREWES 1996 Research Report

Stewart, R., Ferguson, R., Miller, S., Gallant, E., and Margrave, G, 1996, The Blackfoot Seismic Experiments: Broad-band, 3C-3D, and 3D VSP surveys, CSEG Recorder (June 1996)

Yang, G. Y. C., Lawton, D. C., Stewart, R. R., Miller, S. L. M., Potter, C. C., Simin, V. C., 1996, Interpretation and Analysis of the Blackfoot 3C-3D Seismic Survey: CREWES 1996 Research Report

Yilmaz, O., 1987, Seismic Data Processing, Society of Exploration Geophysicists

APPENDIX

The spectral estimation software used to examine the Blackfoot surveys is included in the 1996 software release to the sponsors (Foltinek and Bland, 1996). The software is written in Matlab and consists of two programs, *seisimage* and *fxtran*.. *Fxtran* calculates the f-x spectrum of an input seismic data set and returns the 'complex phase' spectra and amplitude spectra. It is purely a numerical computation routine, while *seisimage* uses an interactive display which incorporates *fxtran*. The user interface is shown in figure A1 with the pull down menu and both pop-up windows. The seismic data set, in time, is displayed in the main window.

To use *seisimage* , start at the bottom of the 'tools' pull down menu by choosing, 'Set tool space/time zone'. This creates a pop-up window in which the time and distance coordinates specifying time window for the calculations can be entered. To close the pop-up window, select 'Done'. Next, choose 'Set fxtran parameters' from the 'tools' menu. This also creates a pop-up window for user input. The percentage taper and random fluctuation in length of the time window can be specified, as well as the maximum frequency of the final spectra displays and type of section desired. The 'Window Type' options is not functional in this version. The final step is to select 'fxtran', from the 'tools' menu. This button calls the routine, *fxtran* to perform the calculations and create the spectral display plots.

Although the two programs will ultimately create the same display, *seisimage* has two main advantages over using *fxtran* alone. First, the user can specify the windows and parameters while viewing the seismic data set in the time domain. Also, several estimates using various windows can be performed without leaving the *seisimage* display.

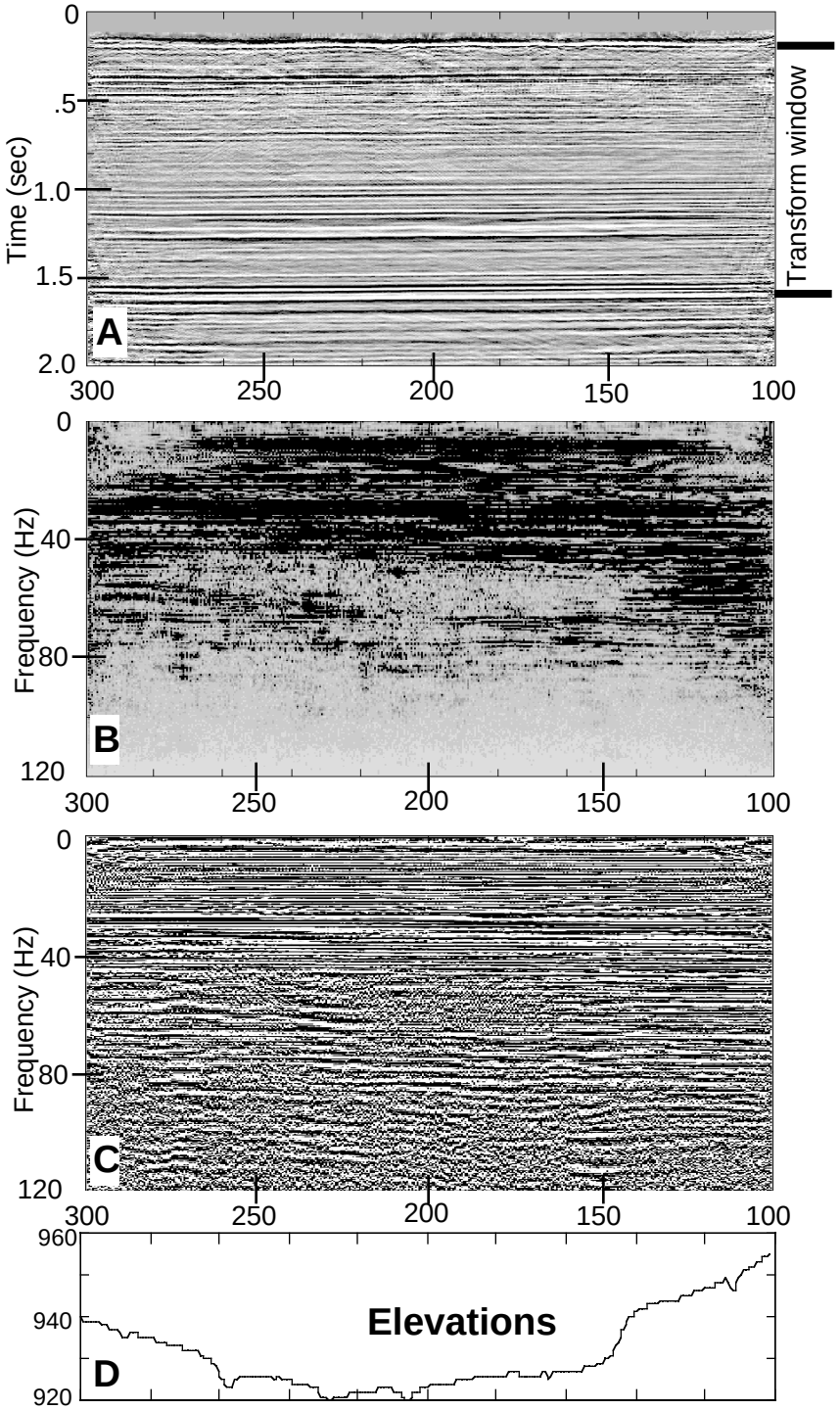

Figure 1. The final stack for the Blackfoot 2D 10 Hz array data (A) (Blackfoot 2D) and its f-x spectral analysis. The amplitude spectrum (B) and the complex phase spectrum (C) were computed over the time zone .2 to 1.6 seconds. Note the spatial correlation of the spectral notch near 55 Hz (beginning at station 140 and extending past 260) and the elevations along the line (D).

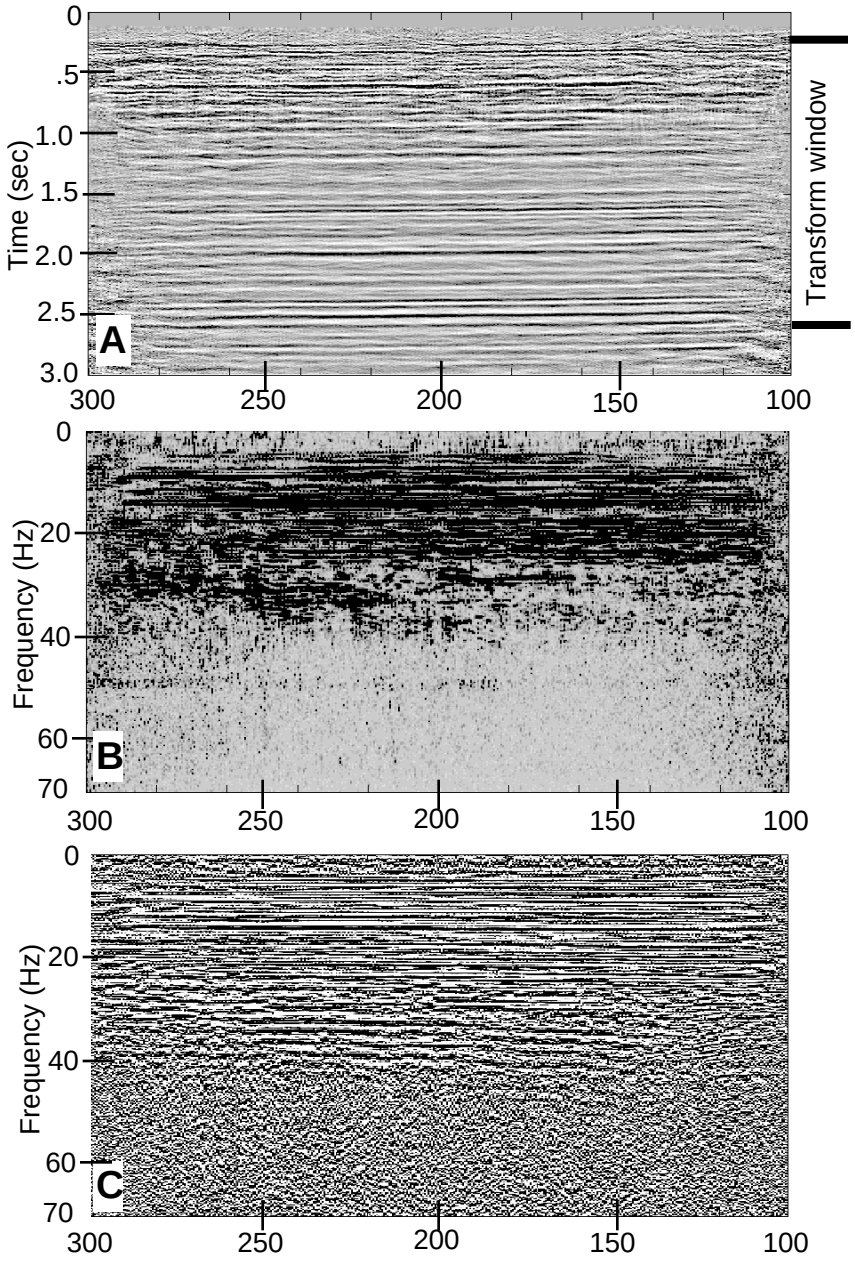

Figure 2. The final stack for the radial component of the Blackfoot 2D 10 Hz 3-C data (A) (Blackfoot 2D) and its f-x spectral analysis. The amplitude spectrum (B) and the complex phase spectrum (C) were computed over the time zone .2 to 2.6 seconds.

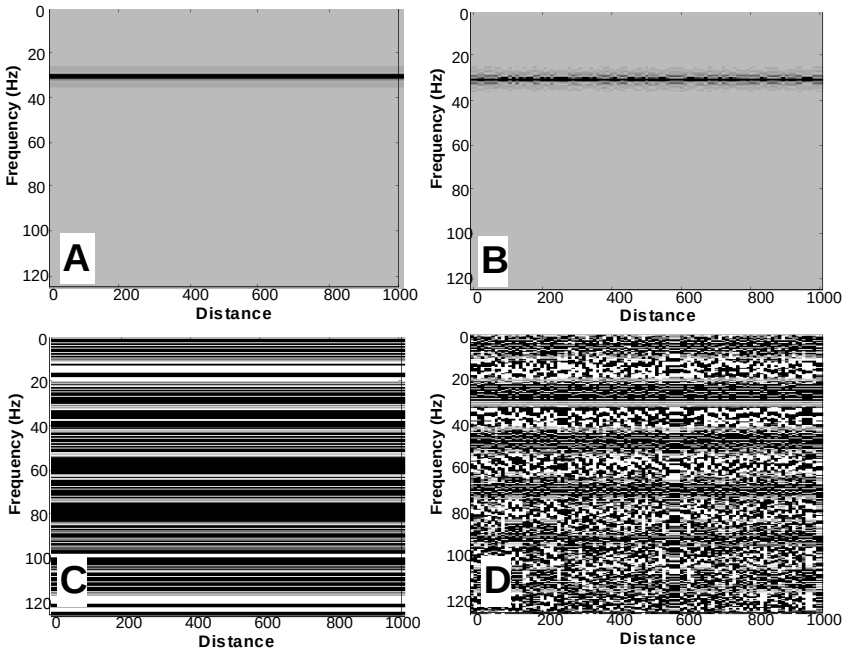

Fig. 3. The input to these f-x spectral analyses was a noiseless, monochromatic (30 Hz) synthetic stack. The left column (A and C) shows results computed with a spatially constant transform window while the right column (B and D) used a randomly variant window. The top row (A and B) are amplitude spectra and the bottom row (C and D) are complex phase spectra.

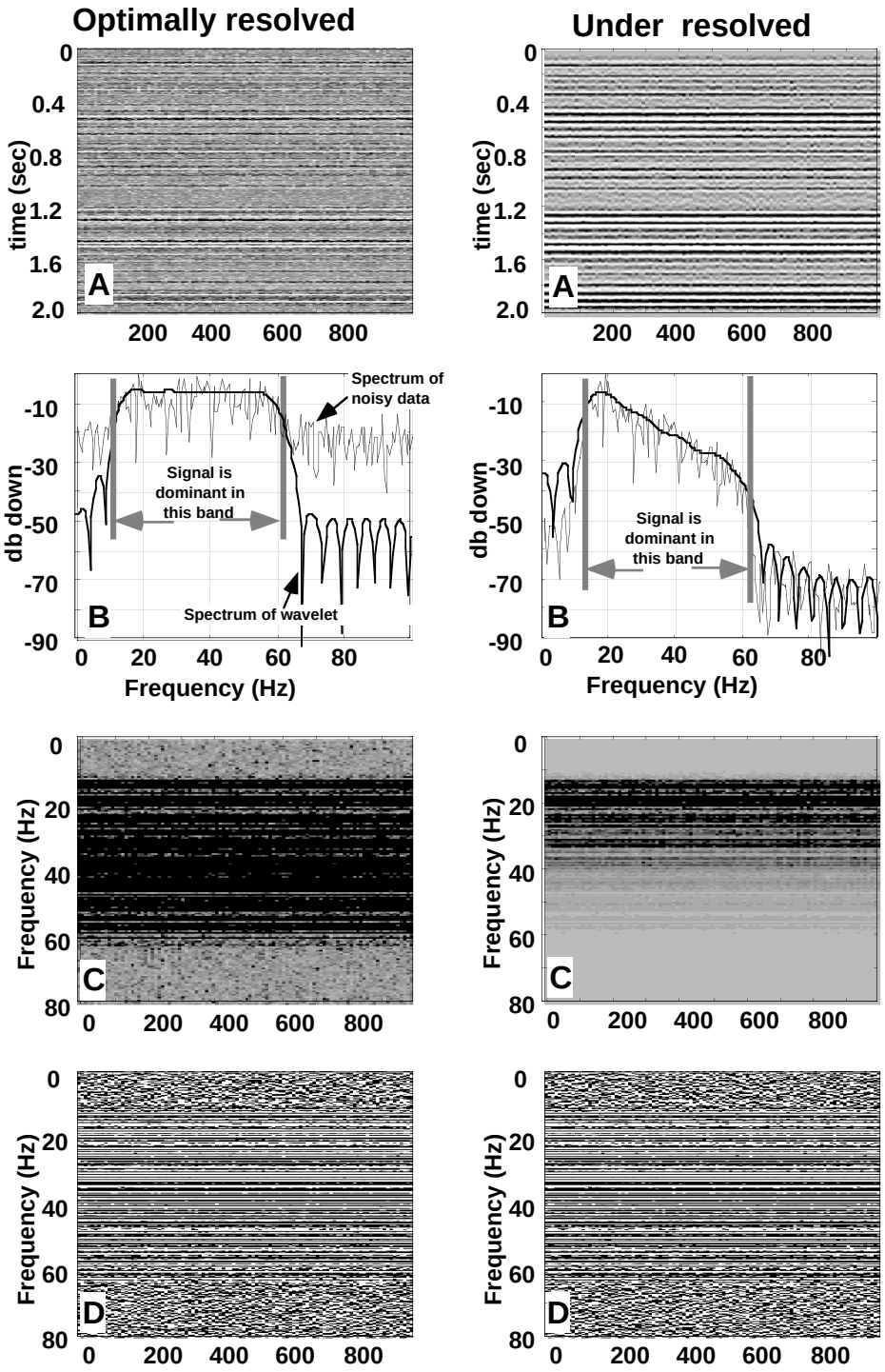

Fig. 4. The f-x spectral analysis of bandlimited synthetics which are "optimally resolved" (left) and "under resolved" (right). Synthetic stacks (A), wavelet and trace spectra (B), f-x amplitude spectra (C), and f-x complex phase spectra (D).

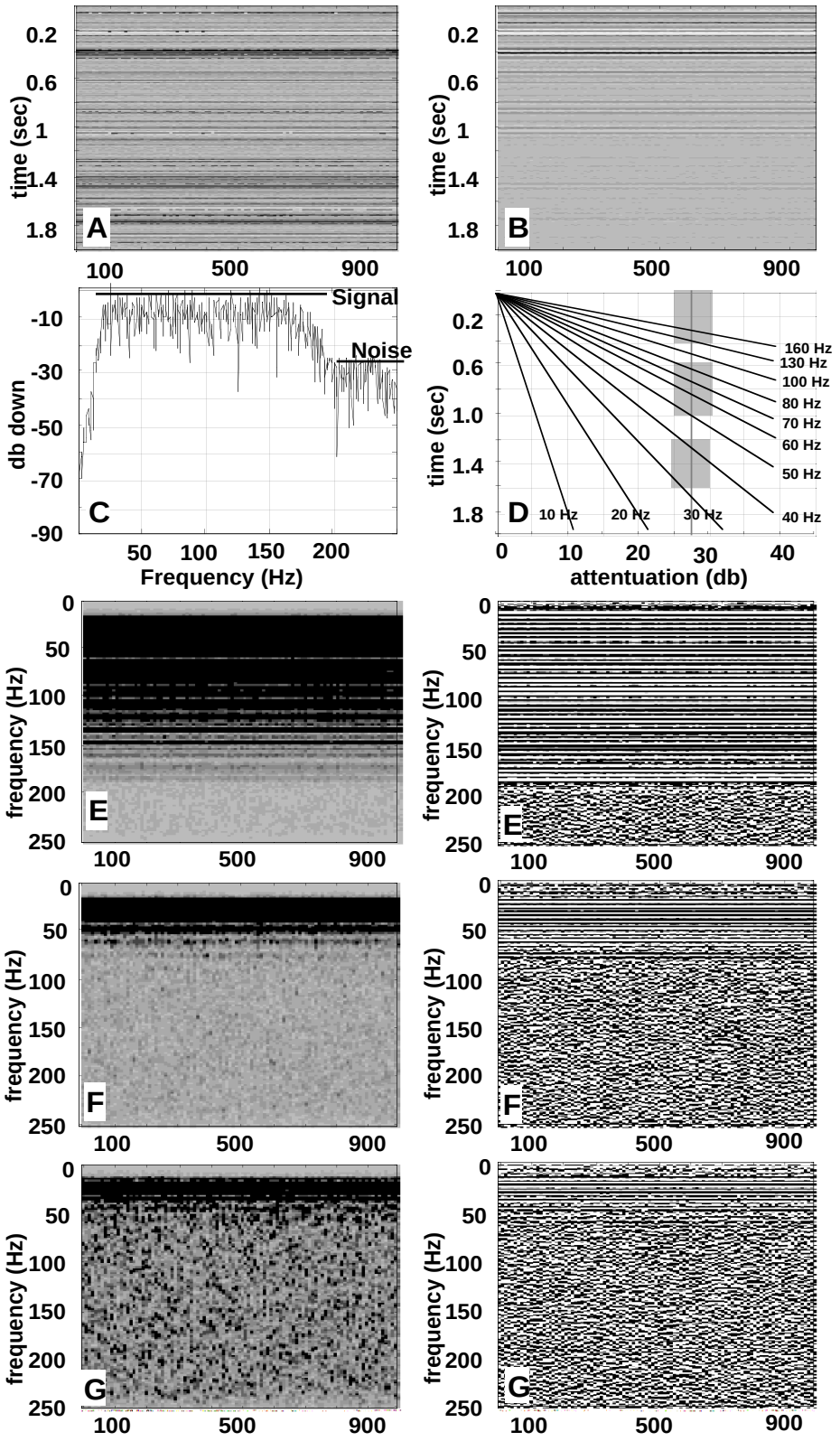

Fig. 5. Analysis of a non-stationary synthetic. Stationary synthetic (A), non-stationary synthetic (B), expected signal of stationary synthetic (C), signal decay curves and expected signal of non-stationary synthetic (D), f-x analysis of (B) from 0 to .4 seconds (E), f-x analysis from .6 to 1.0 seconds (F), f-x analysis from 1.2 to 1.6 seconds (G)

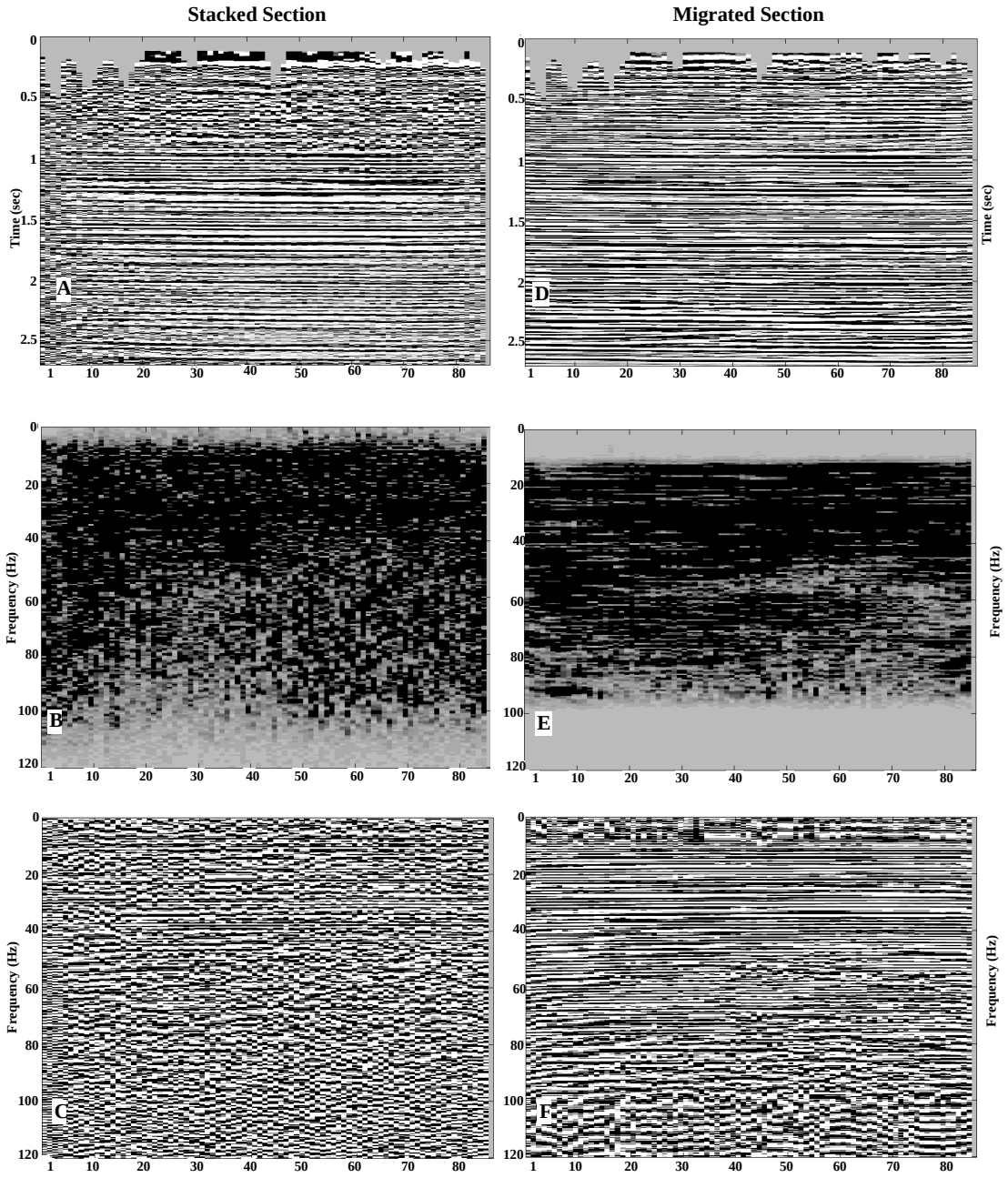

Fig. 6. The final stack (A) and migrated section (D) of the Blackfoot 3C-3D P-P data, processed by Sensor, and their f-x spectral analyses. The amplitude spectra (B and E) and the complex phase spectra (C and F) were computed over the time zone of 0.2 to 1.6 seconds.

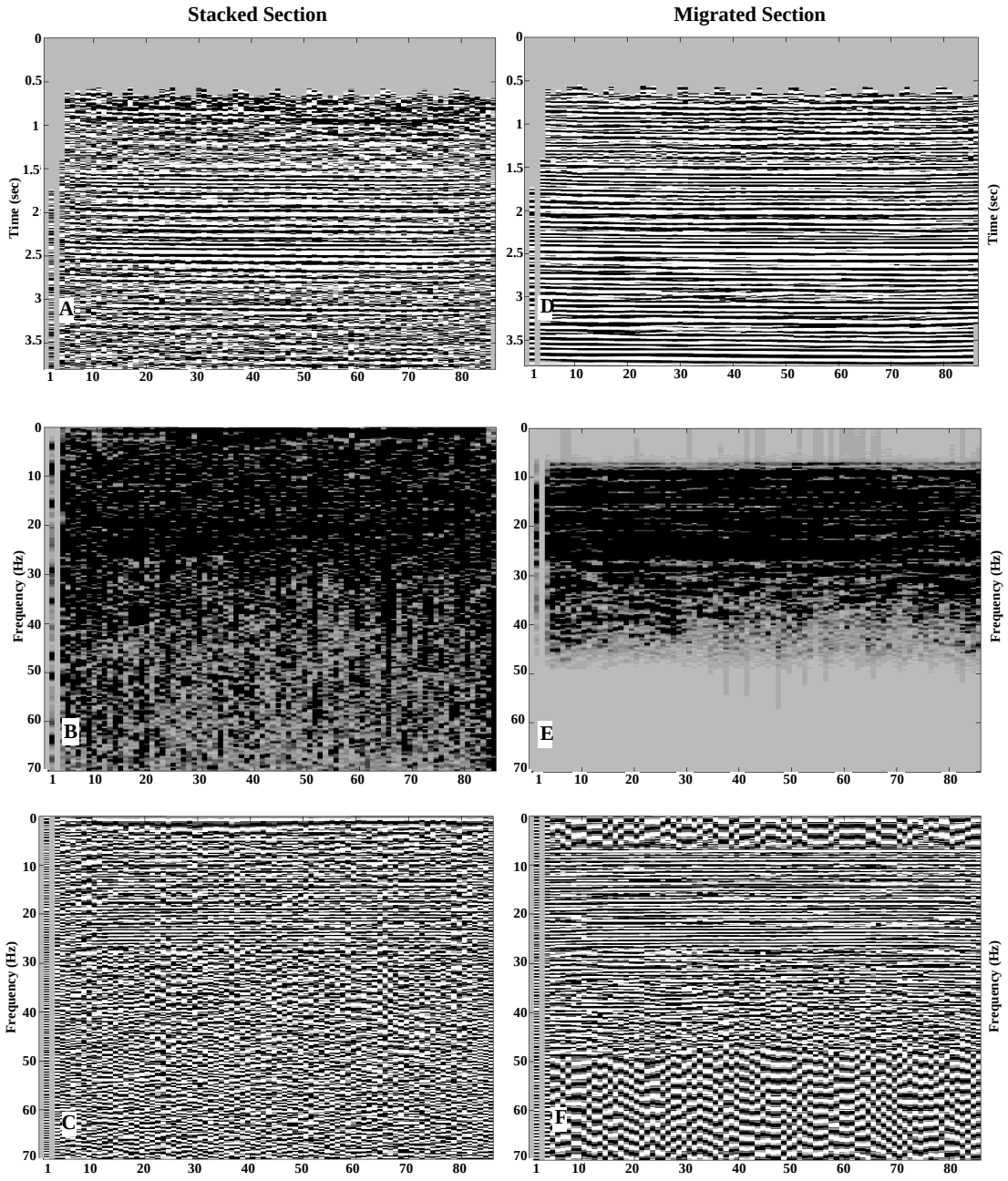

Fig. 7. The final stack (A) and migrated section (D) of the Blackfoot 3C-3D P-S data, processed by Sensor, and their f-x spectral analyses. The amplitude spectra (B and E) and the complex phase spectra (C and F) were computed over the time zone of 0.2 to 2.6 seconds

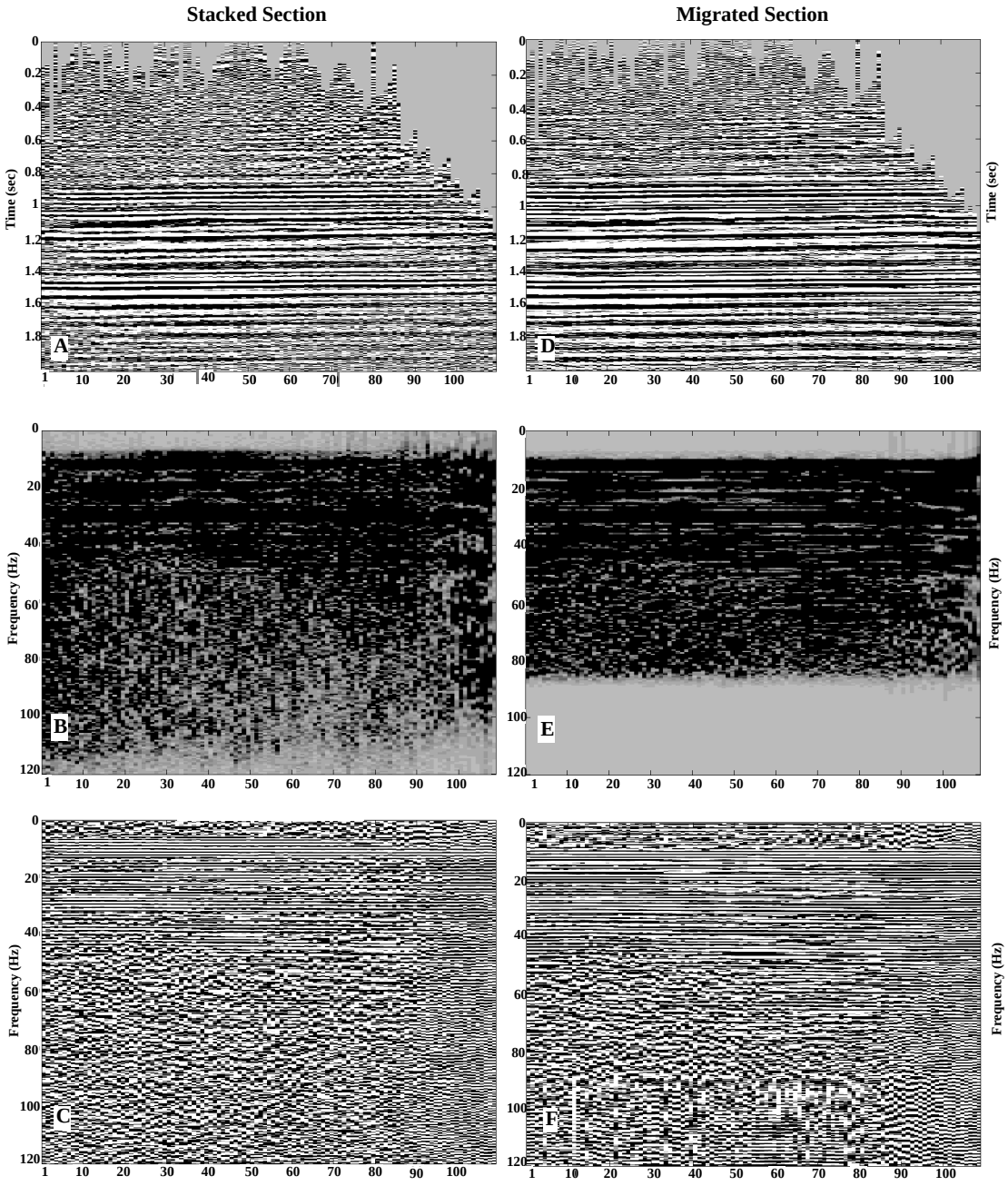

Fig. 8. The final stack (A) and migrated section (D) of the Blackfoot 3C-3D P-P data, processed by Pulsonic, and their f-x spectral analyses. The amplitude spectra (B and E) and the complex phase spectra (C and F) were computed over the time zone of 0.2 to 2.6 seconds

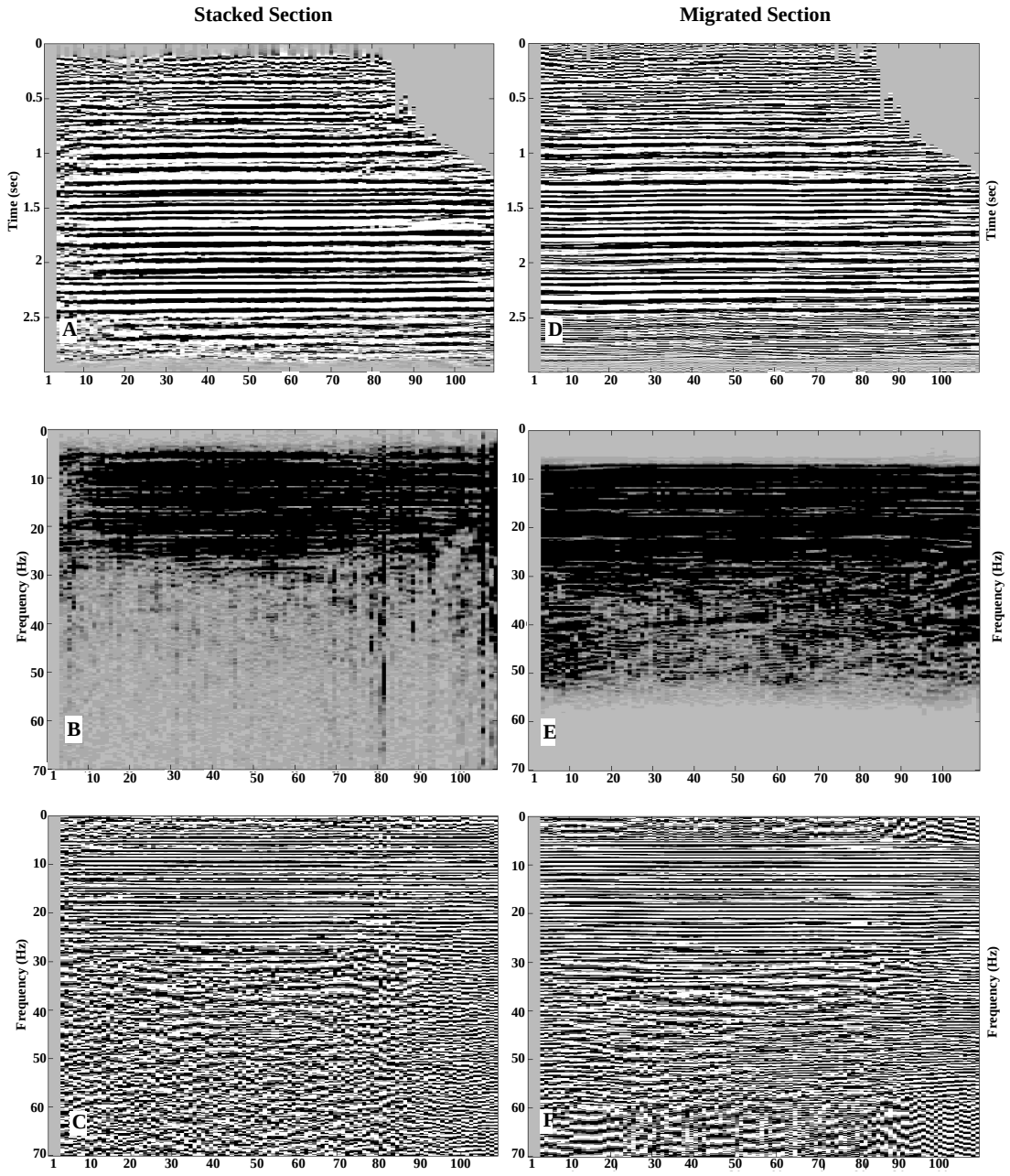

Fig. 9. The final stack (A) and migrated section (D) of the Blackfoot 3C-3D P-S data, processed by Pulsonic, and their f-x spectral analyses. The amplitude spectra (B and E) and the complex phase spectra (C and F) were computed over the time zone of 0.2 to 2.6 seconds

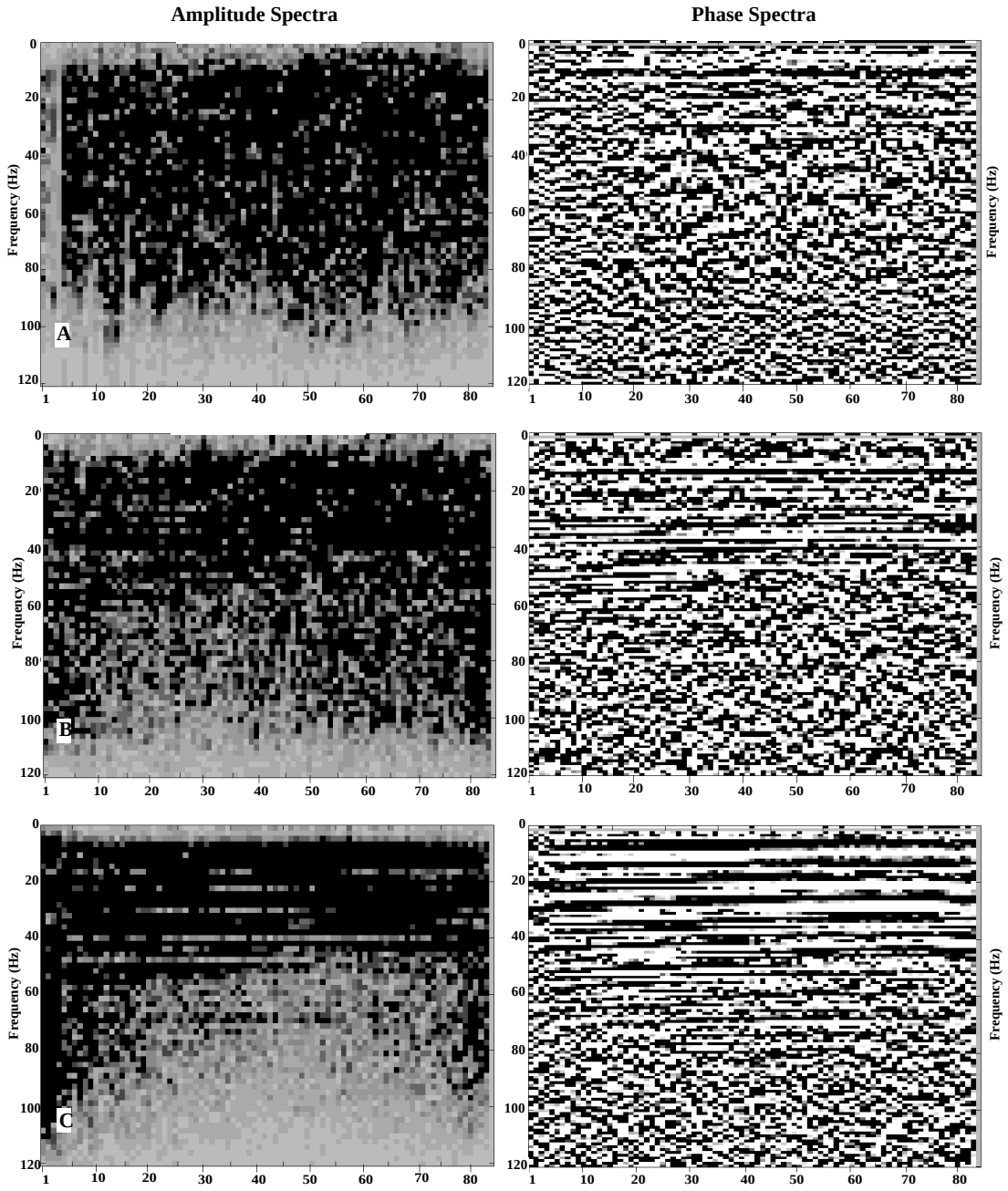

Fig. 10. F-x spectra from three different windows on stacked P-P data, processed by Sensor

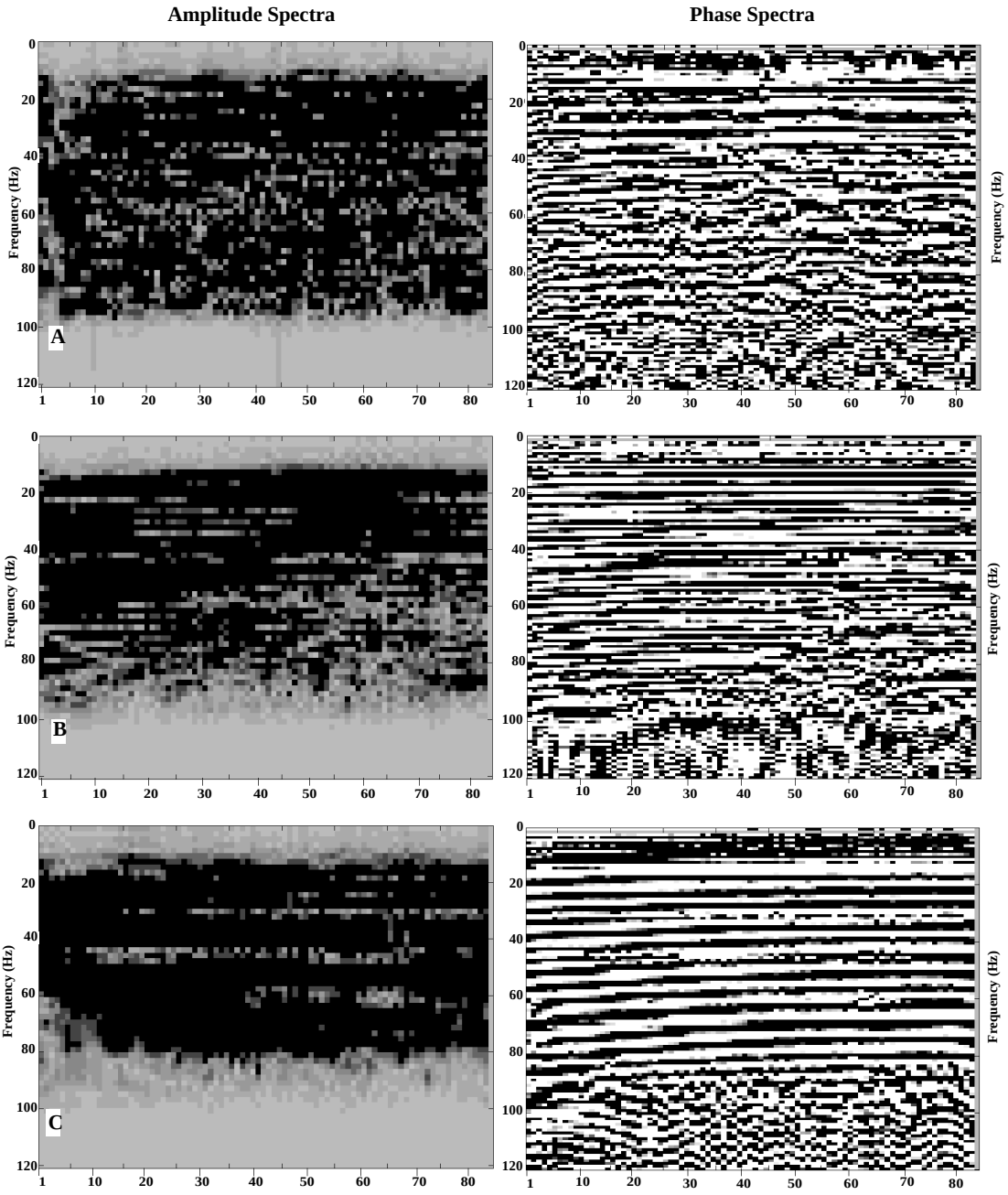

Fig. 11. F-x spectra from three different windows on migrated P-P data, processed by Sensor

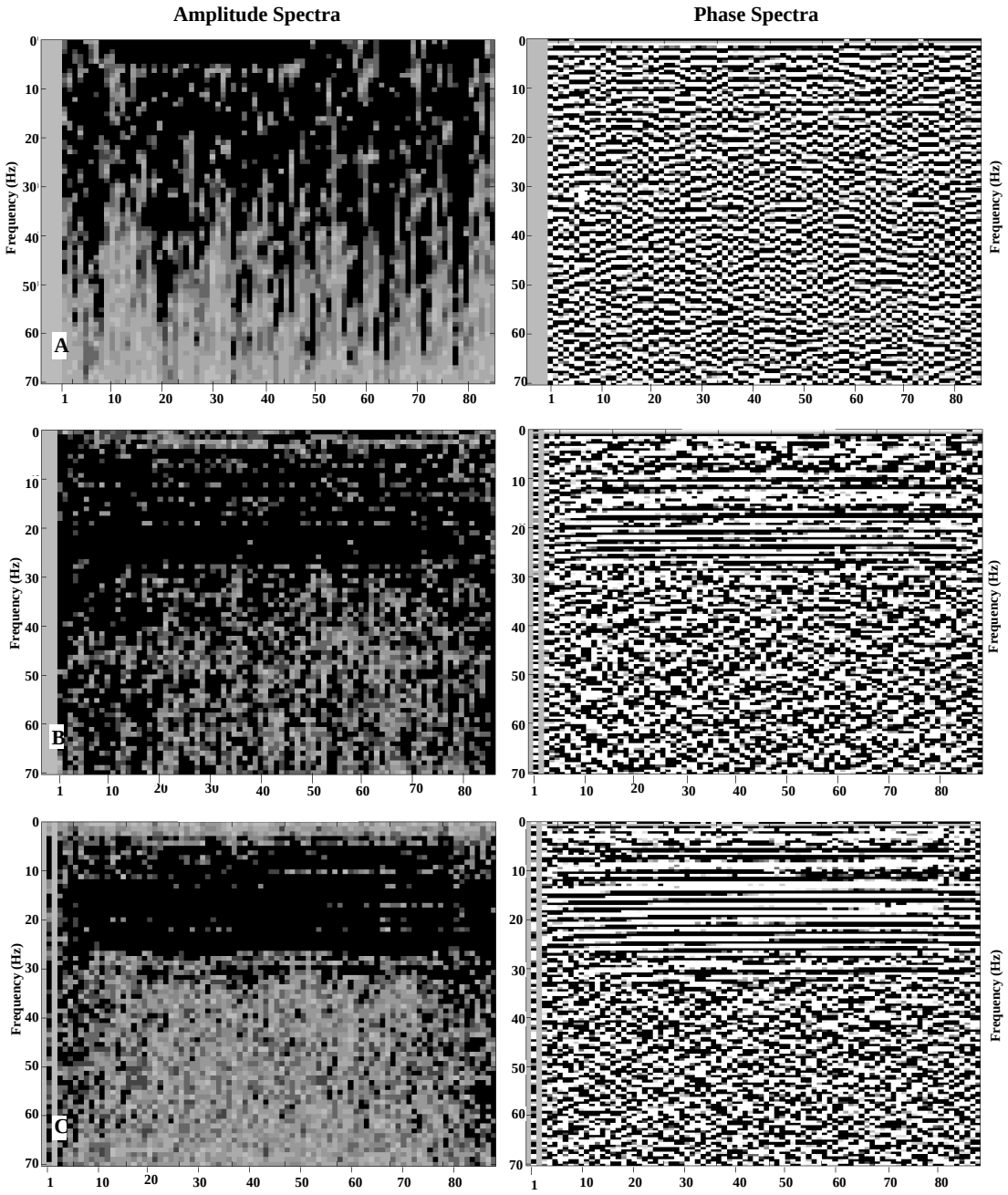

Fig. 12. F-x spectra from three different windows on stacked P-S data, processed by Sensor

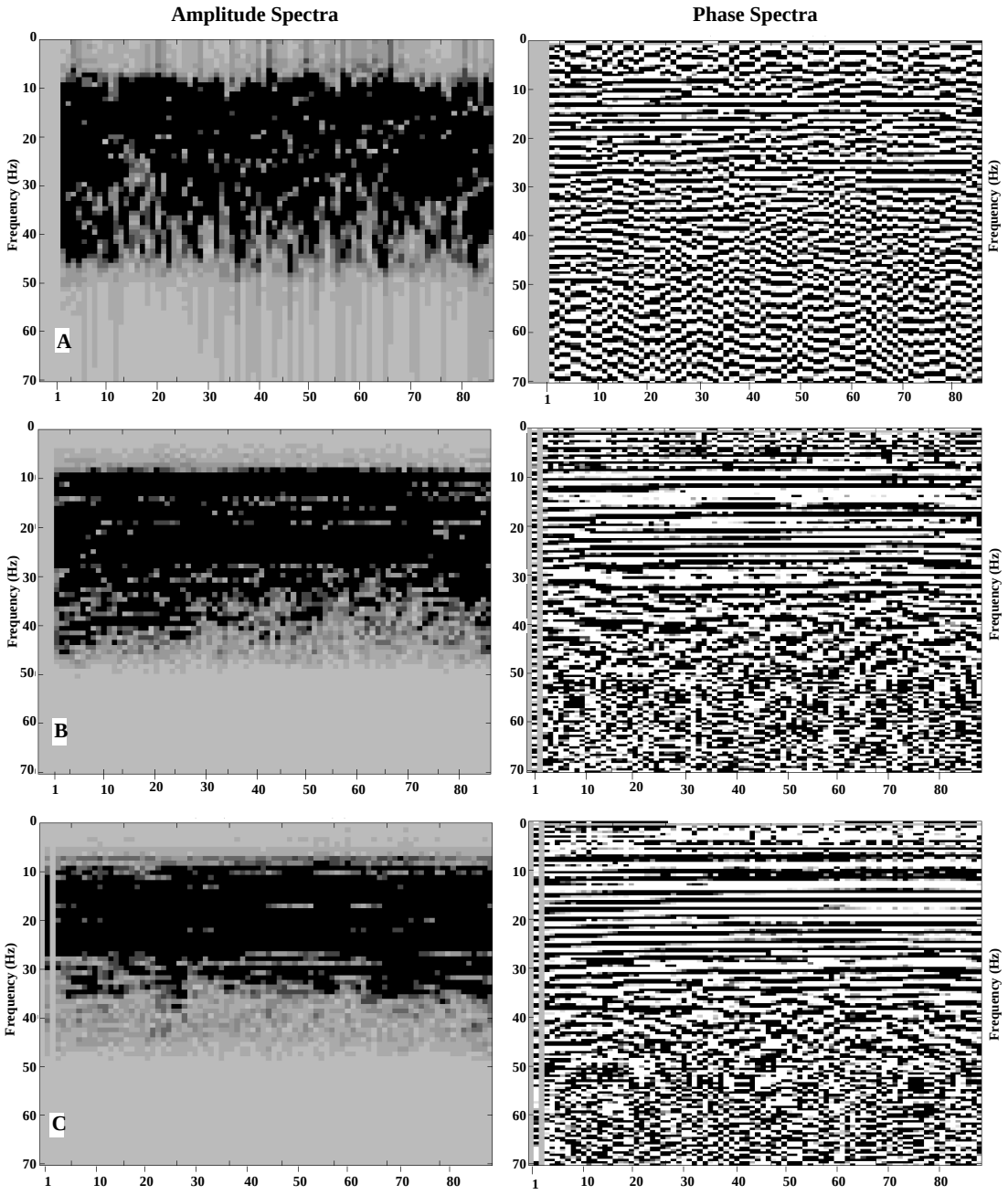

Fig. 13. F-x spectra from three different windows on migrated P-S data, processed by Sensor

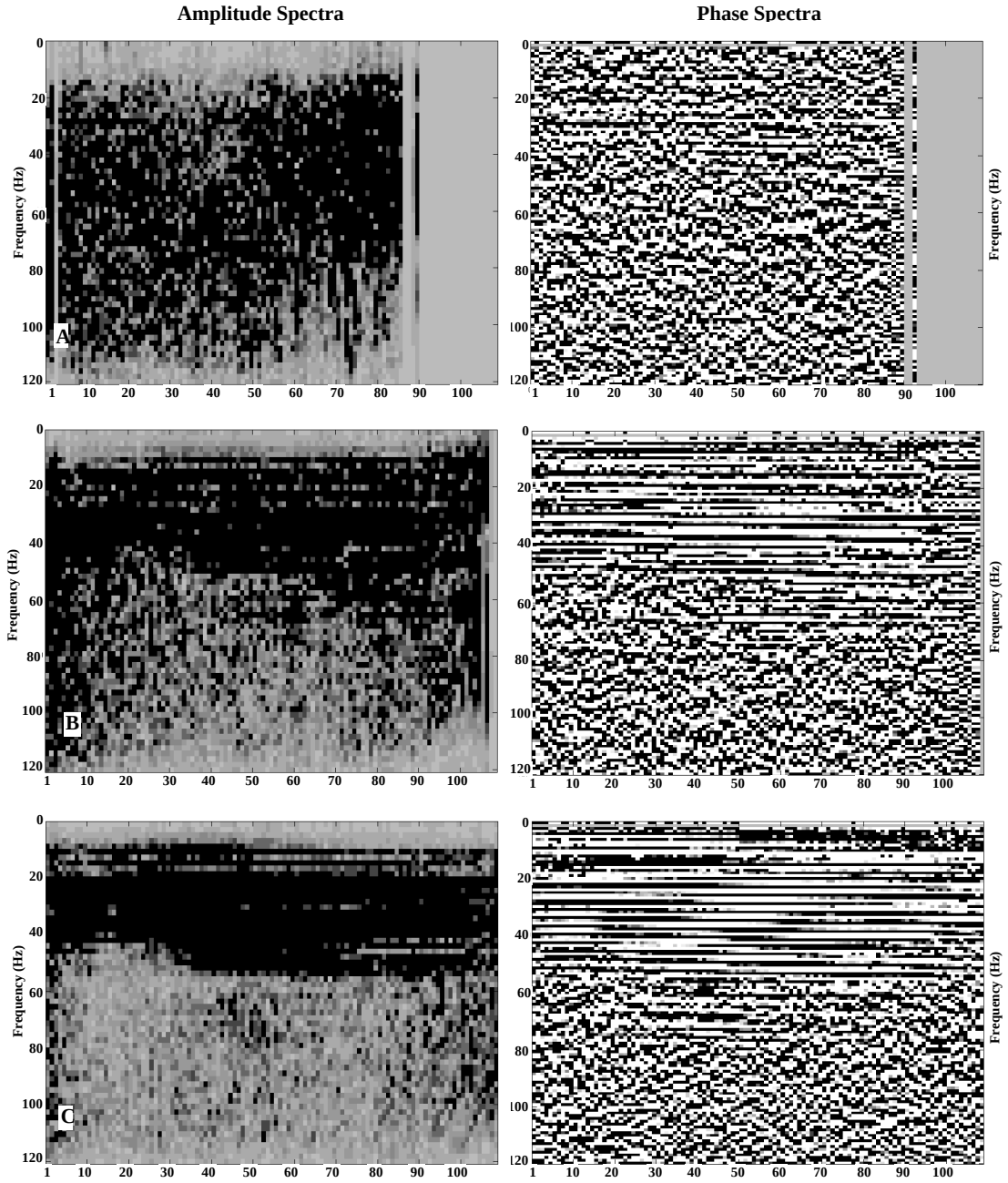

Fig. 14. F-x spectra from three different windows on stacked P-P data, processed by Pulsonic

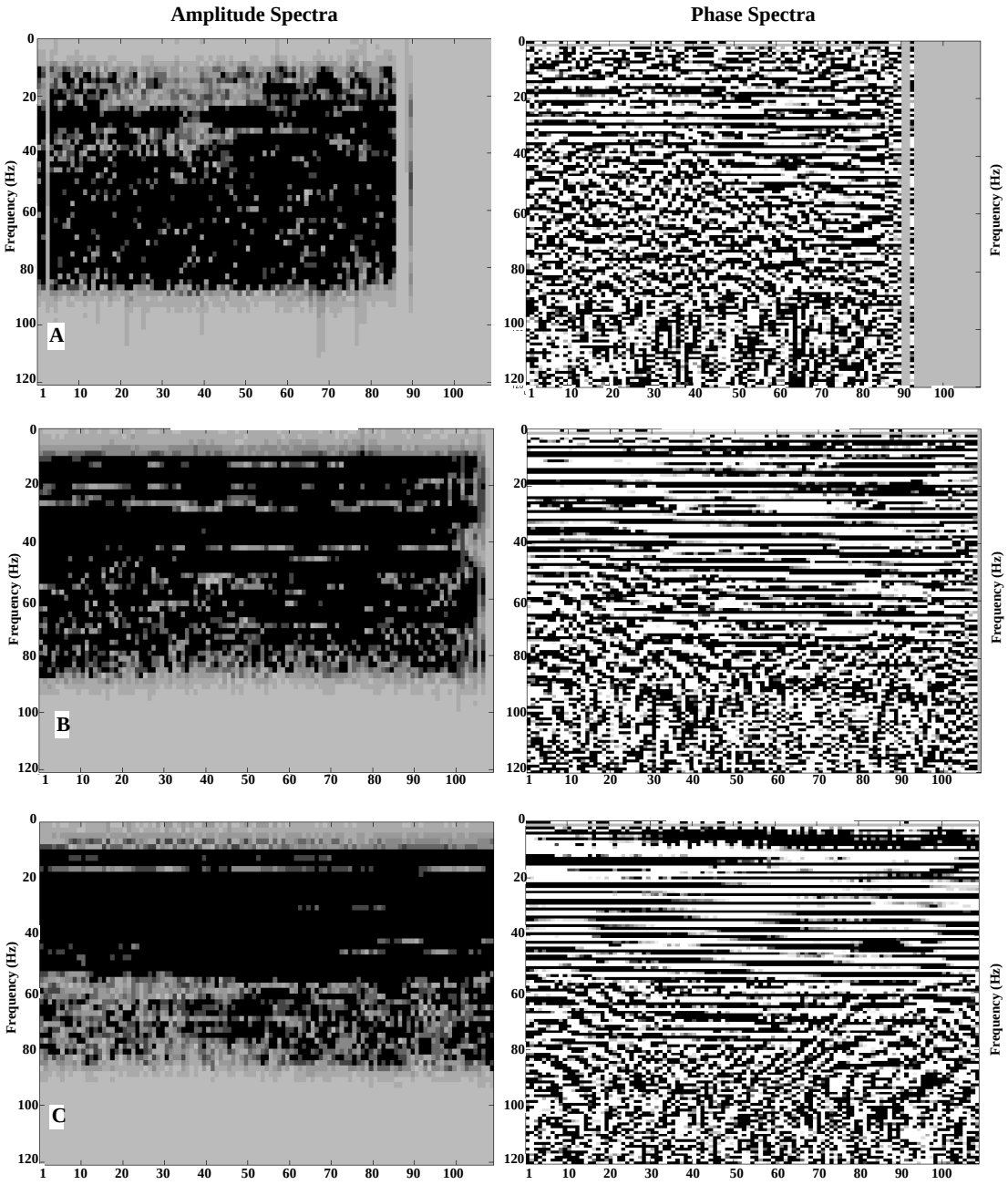

Fig. 15. F-x spectra from three different windows on migrated P-P data, processed by Pulsonic

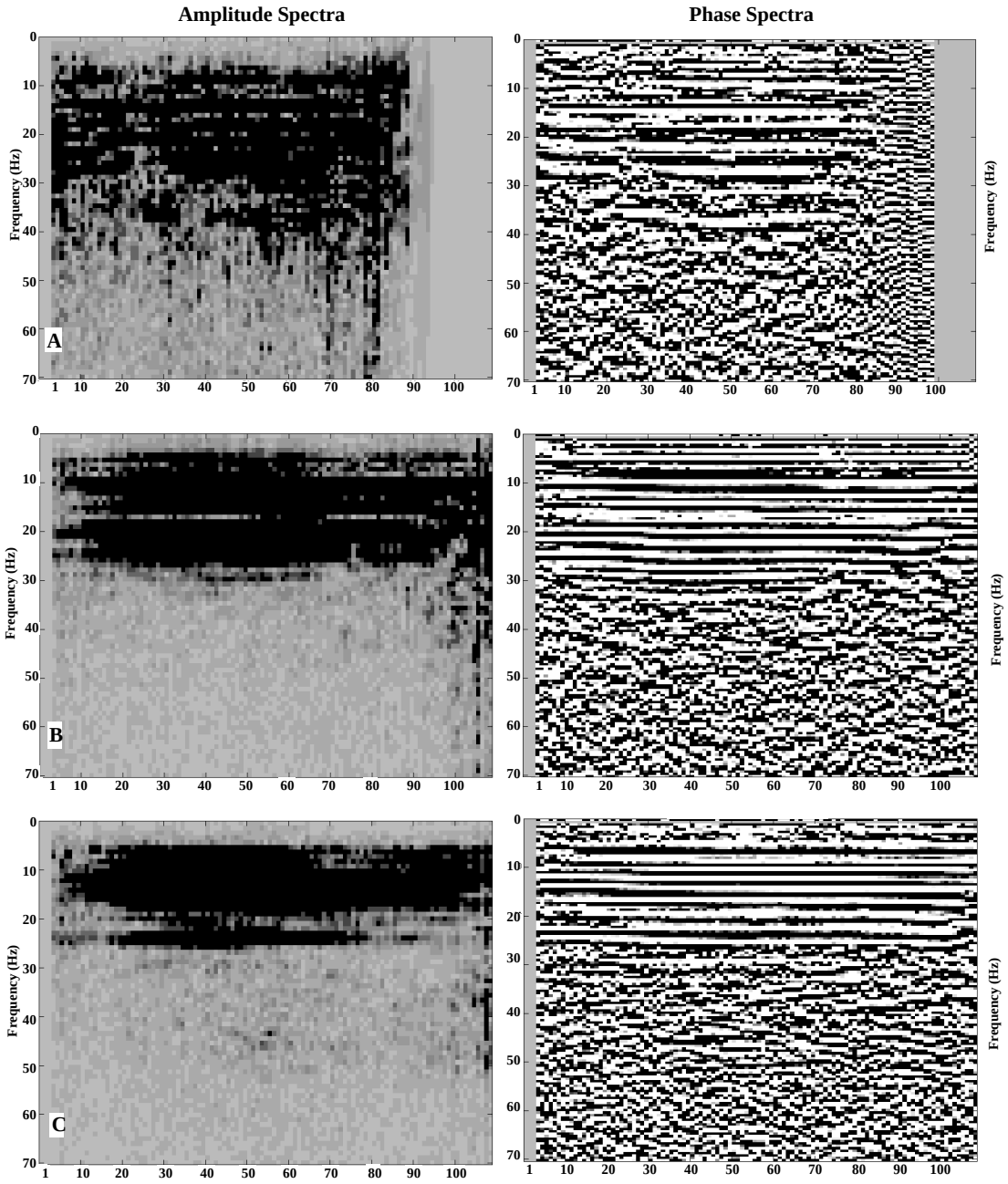

Fig. 16. F-x spectra from three different windows on stacked P-S data, processed by Pulsonic

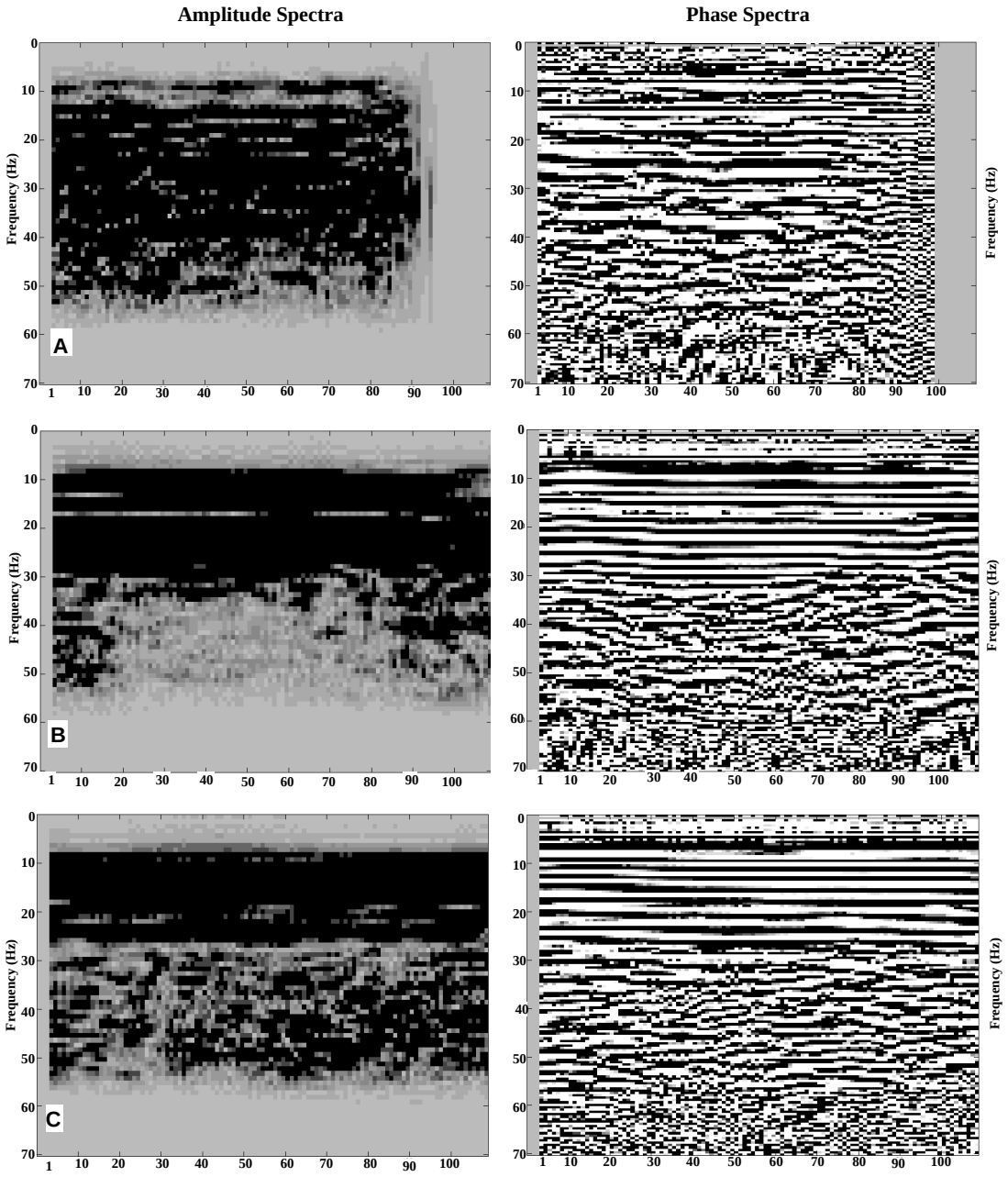

Fig. 17. F-x spectra from three different windows on migrated P-S data, processed by Pulsonic

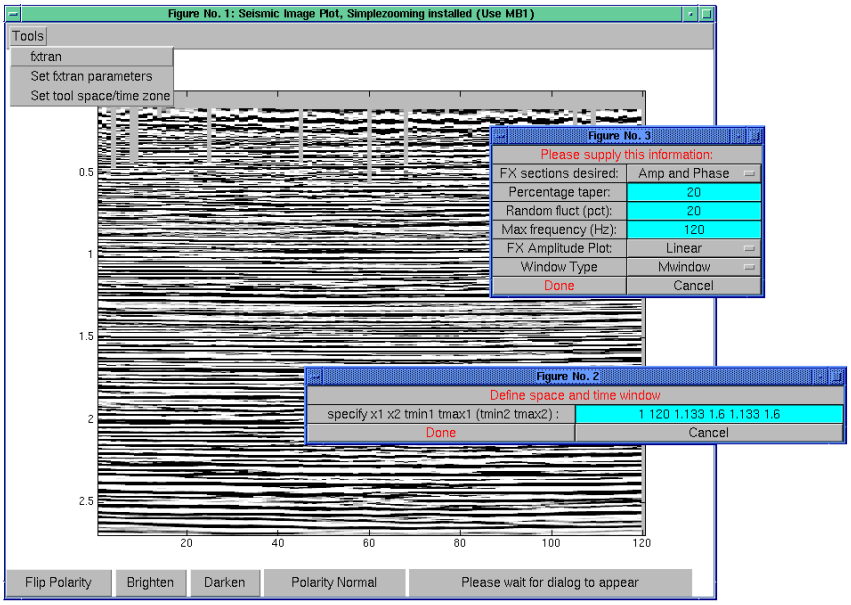

Fig. A1 The GUI for the *seisimage* routine, showing the pull-down menu and pop-up windows